Process modelling of the laser treatment of titanium with aluminum

Conference Paper · June 1992

CITATIONS
0

READS
7

1 author:

Jaafar Hadi Abboud
University of Babylon
34 PUBLICATIONS **663** CITATIONS

SEE PROFILE

η_t), and by increase of cut width b. As well it brings the periodicity in destruction process which results in striation formation on cut surface. More so for speed lower then Vo the increase of exothermal burning reaction in general energy balance is observed (the increase of Rm coefficient). As a result at very low cutting speed the exothermal reaction energy is enough to sustain the spontaneous destruction process which is observed experimentaly. Cutting at speed higher then Vo is taking place if the released heat in cut cavity is not enough to distroy the whole needed material mass and entire sharing of the metal plate wouldn't occur. To check the theoretical data the experimental study using planning of experiments methodics have been performed.

As quality cut parameters the cut width (b), surface roughness (Rz) and dross hight at lower edge of cut (Hg) were used.

As a result of theoretical and experimental data comparison it was found that the developed model fit the GLC process adequately (Figure 3). Analysis shows that dross hight has straight connection with melt thickness on destruction surface. The relative divergence of optimum points for these two dependences constitutes about 12% (Figure 4). Therefore the found theoretical dependence of melt thickness may be used to evaluate the dross height.

5. Conclusions

Based on the analysis of metals GLC mechanisnm as a result of two interconnected heat exchange and mass transfer processes the new mathematical model for this machining method have been developed. Computated dependences of the model are obtained as a result of different GLC process theoretical conceptions generalization. There is quite sufficient correspondence between the cutting parameters calculated using the model and the experimental data. This allows to recommend the developed model to predict the optimal metal materials cutting conditions.

6. Nomenclature explanation

A — liquid layer absorptivity;
A_m — metal absorptivity;
P — laser radiation power;
P_{ch} — exothermal reaction power;
P_h,P_m,P_v — power expenditures on metal heating up to the destruction temperature, on melting and evaporation, correspondingly;
M_m — melt mass on the border of phase change;
M_{ch} — material mass, which takes part in exothermal reaction;
M_g,M_v — mass losses as a result of melt metal removal by gas flow and by evaporation;
ρ,C — material specific heat;
λ , a — heat- and temperature conductivity of material;
r_0 — Gussian radius of laser power density distribution;
h — cut metal thickness;
b — cut width;
ϑ — cutting speed;
To — destruction surface temperature;
Hm, Hv — specific heat of melting and evaporation;
G_{ch} — specific heat of burning reaction;
E_i — exponential integral;
E, T_* — evaporation constants;
S — liquid layer thickness;
δ,T_δ— diffusion activation process constants;
α_1 — constant, dependent on oxide properties;
p — excessive pressure of gas flow in cut cavity;
η — melt dynamic viscosity;
ρ_g,η_g,V_g — gas flow density, dynamic viscosity and speed;
ρ_g^*,η_g^* — gas characteristics in dynamic state;
V — melt phase volume;
τ^*,δS,K, ω — integral constants.

7. References

[1] V. S. Kovalenko, V. V. Romanenko and L. M. Oleschuk: "Advanced Processes of Cutting with Laser Beam," p.112; Technica, Kiev, 1987 (in Russian).
[2] W.Schulz: "On Laser Fusion Cutting up Metals,: I. Phys. D.: Applied Physics, 20 (1987) p.p.481-488.
[3] W. Duley: "Processing and Analysis of Materials," p.504, "Mir", Moscow, 1986 (in Russian, translated from English).
[4] A. M. Prochorov, at all: "Laser Radiation Interaction with Metals," p.615.; "Nauka", Moscow, 1988 (in Russian).
[5] M. Vicanek, at all: "Hydrodynamical Instability of Melt Flow in Laser Cutting," I. Phys. D.: Applied Physics, 20, (1987) p.p.140-145.

Process Modeling of the Laser Surface Treatment of Titanium with Aluminum

Roger C. REED, J.A. ABBOUD and D.R.F. WEST

Department of Materials, Imperial College, Prince Consort Road, LONDON SW7 2BP, U.K.

1. Introduction

Ordered intermetallic titanium aluminide alloys are emerging as attractive materials for high temperature structural applications, particularly for the aerospace industry. The advantages of these alloys over conventional nickel-based superalloys or titanium alloys include: high specific modulus, high recrystallisation temperatures, and low self diffusion, which leads to improved high temperature creep and oxidation resistance [1,2]. Such properties potentially permit higher operating temperatures for aerospace engines, and in turn higher thrust/weight ratios, improved operating efficiencies and fuel savings [*e.g.* 3]. The research seems to have reached the stage where potential applications are being actively sought; these lie in hypersonic airframes, and many aeroengine components in the immediate (IP) and high pressure (HP) compressor, combustor outer casing, HP outlet guide vanes, HP turbine seal support and tail bearing housing [4].

However, use of these alloys for these potential applications is restricted at present by poor toughness, ductility and resistance to fatigue, particularly at room temperature. Ti_3Al (α_2) currently shows 2-3% and TiAl (γ) 0.5% elongation at room temperature, although these figures can be improved by alloying additions (such as carbon [5] and niobium [6]) to the binary alloys. This brittleness makes fabrication, handling and shipping at ambient temperatures difficult, and means that component failure during engine start-up is a possibility. At the operating temperatures envisaged, use of fracture mechanics for the evaluation of the fatigue life of such components indicates that the projected lifetime is prohibitively short; many of the components listed above must never fail in service due to the catastrophic effects on engine integrity.

An alternative approach, which might largely circumvent the above problems, involves the in-situ production of titanium aluminide surface zones on titanium substrates using laser processing. Advantage could then be taken of the improved oxidation resistance of the aluminide phases, perhaps in regions which locally are subjected to higher operating temperatures than the rest of the component. Recent work [7,8,9] has shown that this approach is technically feasible; the approach involves spraying aluminium powder under a stream of argon into a laser melted pool of titanium, for a range of processing conditions.

However, if the process is to be industrially viable, it is vital to be able to produce the desired composition and dimensions of alloyed zones in a repeatable way. The process variables (such as traverse speed, powder feed rate, laser power and distribution) must be optimised, and then carefully controlled. Process modelling can help, by identifying the critical process variables. It can also give a measure of the sensitivity of the composition and dimensions to the process variables. In this work, recent experimental results are analysed critically in an effort to produce input data for a mathematical model for the process. Progress in the development of a mathematical model for the process is reported.

2. Experimental Procedure

The experimental procedure [7,8,9] for the surface alloying of aluminium into titanium substrates has been reported already, and so will only be briefly summarised here. A 2 kW CW CO_2 laser operating at 1.8kW, with a beam diameter of 3 mm was employed throughout the course of these experiments. To supplement the existing experimental data [7,8,9] further experiments were carried out in an identical manner. These included a series of experimental runs in which the Al feed rate was set to zero (the degenerate case of laser surface melting). As will be seen, the simple case of surface melting is required for the calibration of the mathematical model developed.

The power distribution in the laser beam was established using a hollow needle beam analyser [10]. Commercial purity Al powder (100 μm average particle size) was blown using argon gas into the melt zone of Ti. Analysis of the alloyed zones showed that the oxygen content of the alloyed regions was only marginally greater than that of the substrate, and therefore that the shrouding system was effective. Cracking was observed only at the highest aluminium contents (of the order of 80 at%). The porosity detected was negligible. The dimensions of the laser surface alloyed zones were determined by examination of transverse sections, using a travelling microscope. Scanning electron microscopy (SEM) with a capability for energy dispersive spectrometry (EDS) was used to determine the chemical composition of the alloyed zones.

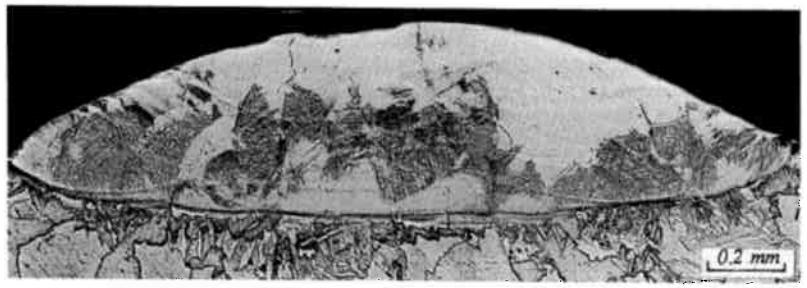

Figure 1: Example of Ti substates laser surface alloyed with Al.

SPEED /(mm/s)	FEED RATE /(g/s)	WIDTH w /mm	DEPTH d /mm	HEIGHT h /mm	COMPOSITION /at%
20.0	0.055	1.2	0.13	0.05	22
20.0	0.070	1.3	0.07	0.13	43
20.0	0.081	1.4	0.15	0.15	58
15.0	0.055	1.4	0.20	0.10	22
15.0	0.070	1.6	0.17	0.18	43
15.0	0.081	1.75	0.20	0.20	58
10.0	0.055	1.8	0.23	0.12	22
10.0	0.070	2.15	0.25	0.20	43
10.0	0.081	2.2	0.27	0.28	59
7.0	0.055	2.3	0.27	0.18	22
7.0	0.070	2.4	0.25	0.30	45
7.0	0.081	2.6	0.22	0.38	62
5.0	0.055	2.55	0.28	0.30	40
5.0	0.070	2.75	0.10	0.60	58
5.0	0.081	2.8	0.15	0.65	65
3.0	0.055	2.75	0.14	0.58	52
3.0	0.070	2.8	0.09	0.76	70
3.0	0.081	2.9	0.12	0.80	75
22.0	0	1.21	0.05	0	0
22.0	0.04	1.28	0.21	0.04	6
17.0	0	1.39	0.08	0	0
17.0	0.04	1.43	0.23	0.06	9
11.6	0	1.46	0.15	0	0
11.6	0.04	1.59	0.26	0.09	9
7.1	0	1.88	0.18	0	0
7.1	0.04	2.01	0.35	0.15	18
3.9	0	2.03	0.44	0	0
3.9	0.04	2.46	0.42	0.24	38

Table 1: Results of the laser surface alloying experiments

3. Experimental Results

Figure 1 shows an illustrative example of the laser surface alloyed zones for the operating conditions employed. In all cases reported the fusion boundary was Gaussian in shape, indicating that the experiments were performed in the conduction/convection-limited (rather than the keyholing) regime. The dimensions of the laser surface alloyed regions, together with the results of the EDS analysis, are tabulated in Table 1. In all cases the EDS analysis indicated that the chemical compositions of the alloyed zones were spatially uniform (to within ± 1 at%). Figure 2 shows the variation of composition of alloyed zone with aluminium feed rate and beam/substrate translation velocity. It is notable that with increasing feed rate, the Al composition increases (as expected); however with increasing translation velocity (at constant feed rate) the Al composition appears to saturate to a constant value. This behaviour needs to be rationalised.

4. Microstructural Observations

The microstructural features of the alloyed zones have been reported by Abboud & West [7]. They noted that for surface alloyed zones of mean composition less than 50%Al (this constitutes a majority of the samples produced), primary solidification to the β phase occurs on cooling. The cooling rate was then sufficiently rapid to produce martensite. With increasing aluminium content, the type and morphology of the martensite changed from lath, to massive/acicular and finally to massive/acicular/lath.

In is considered important to determine more rigorously (in the future) the variation of martensite start temperature with aluminium content, because the martensitic transformation is likely to influence strongly the development of residual stresses in the alloyed zones.

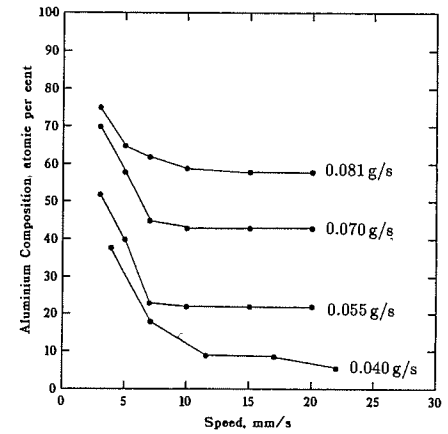

Figure 2: Variation of Al composition of laser surface alloyed zone, with beam/substrate translation velocity and Al feed rate.

5. Numerical Analysis of Experimental Results

Figure 3 is a schematic representation of the alloyed zones produced, and defines terms used here: the width w, height h, depth d, area A_1 (the build-up, or reinforcement) and area A_2 (the area of substrate melted).

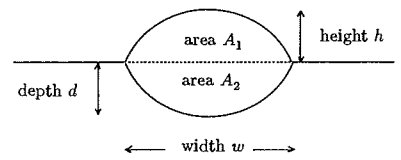

Figure 3: Schematic representation of laser surface alloyed zone.

It is necessary to determine the fraction f of aluminium powder which is alloyed into the melted zones. It is possible to estimate this quantity by noting that it is related to the aluminium feed rate F (mass/time) and the beam/substrate translation velocity v through the approximate relationship

$$A_1 \simeq f\frac{F}{v\rho} \tag{1}$$

where ρ is the density of the aluminium feed powder. This assumes that the alloying of aluminium into molten titanium produces an alloyed zone, the mass of which follows a rule of mixtures. It is probable that the fraction f is a function of F and v (as well as the power distribution of the laser beam) but to a first approximation it is possible to assume that it takes a constant value.

In principle A_1 can be measured experimentally; however the approach taken here involves calculating A_1 using the experimentally determined values of w and h. This involves making an assumption about the *shape* of A_1. As illustrated in figure 3, the assumption is made that A_1 is bounded by an arc of a circle; in this case, defining $a = w/(2h)$ it is possible to show [11]

$$A_1 = \sin^{-1}\left\{\frac{2a}{1+a^2}\right\}h^2\left(\frac{1+a^2}{2}\right)^2 - h^2 a\left(\frac{a^2-1}{2}\right) \tag{2}$$

A similar expression relates w, d and A_2, the cross-sectional area of melted substrate. The quantity f can then be estimated by plotting values of A_1 determined using equation (2) against F/v; from equation (1) this should yield a straight line of gradient ρ/f passing through the origin. Figure 4 shows this plot; the best fit line was determined as $0.0136 \pm 0.0006\,\mathrm{g\,mm^{-3}}$; taking $\rho = 2.7\,\mathrm{g\,cm^{-3}}$ yields $f = 0.20 \pm 0.01$. This value is surprisingly small. Possible errors include loss of aluminium and titanium by vaporisation during

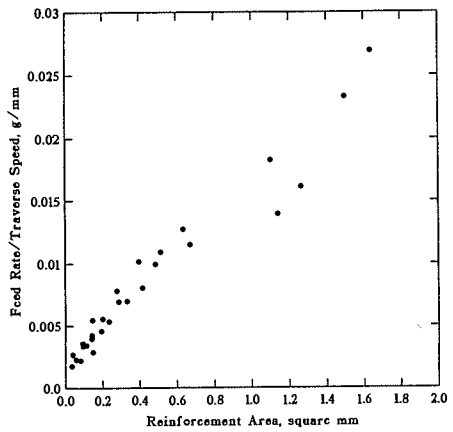

Figure 4: Plot of A_1 (calculated using equation (2)) against ρ/F, to determine f.

processing, inadequacy of the spherical cap geometry, and systematic experimental errors. It should be noted that a value of f could have been determined in a more direct manner by simply weighing the substrate before and after laser processing.

The consistency of the experimental data can be assessed further by noting that the composition (at%) of the alloyed region is given by

$$\text{Aluminium composition} \;=\; A_1/(A_1 + A_2) \tag{3}$$

where A_1 and A_2 can be calculated using experimental values of w, p and h, using spherical cap geometry. Values of $A_1/(A_1 + A_2)$ can then be compared with the compositions determined using EDS analysis. Figure 5 illustrates the result of carrying out this procedure. The experimental data appear to exhibit a high degree of internal consistency, when analysed in this way.

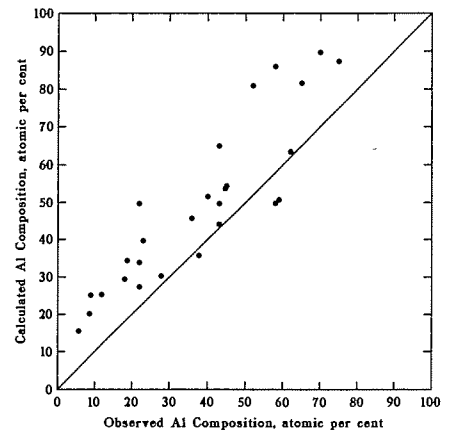

Figure 5: Plot of experimental aluminium composition against the quantity $A_1/(A_1 + A_2)$

For constant laser beam power and power distribution, the area of melting A_2 should vary in a regular fashion with the beam/substrate translation velocity v. Simplified analytical solutions [12,13,14] to the problem of a moving heat source predict $A_2 \propto 1/v$, so that

$$A_2 = \frac{K}{v} \tag{4}$$

where K is a constant. Equation 4 is likely to hold when the ratio F/v is low (the degenerate case of surface melting). However, at some higher value a significant fraction of the incident energy is required to melt the incident aluminium powder, and (4) is likely to fail. The operating regime in which (4) applies needs to be determined.

The validity of (4) has been checked, and the resulting plot appears in figure 6a. Considerable scatter in the data is apparent. However, if the data is restricted to that for which feed rate/velocity $< 0.01\,\text{g/mm}$, the agreement is somewhat improved (figure 6b). The analysis confirms the belief that the ratio F/v is important in determining the efficiency of the laser surface alloying process. However, more experimental work is needed to verify this. Note that no account has been taken of the variation of melting temperature with aluminium composition.

The behaviour noted in figure 1 can be rationalised by combining equations (1), (3) and (4) to give

$$\text{Aluminium composition} = \frac{fF/(v\rho)}{fF/(v\rho) + K/v} \tag{5}$$

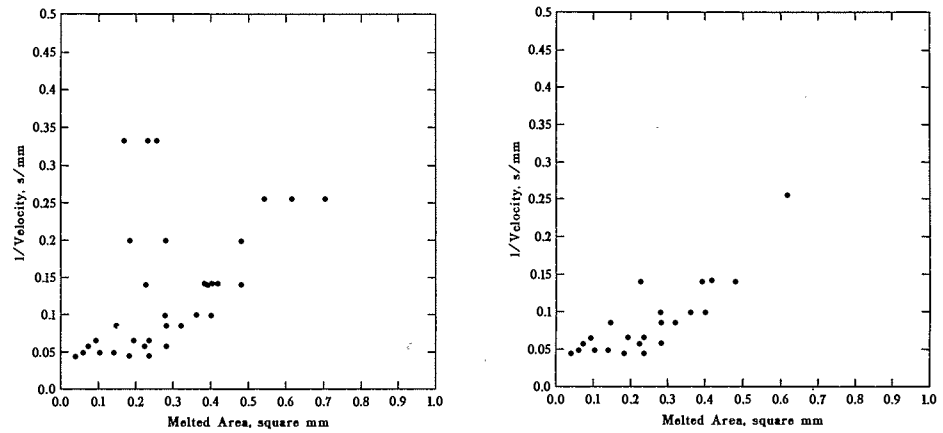

Figure 6: Left, a) Plot of A_2 against $1/v$; Right, b) Plot of A_2 against $1/v$, for $F/v < 0.01\,\text{g/mm}$

an expression which is independent of v. Equation (5) explains the experimental observation that the aluminium composition is independent of F at large v. The critical value of F/v appears to be of the order of $0.01\,\text{g mm}^{-1}$. As already noted, (5) is expected to fail at large F/v.

6. A Model for the Process

The above analysis indicates that, provided that the F/v ratio is low enough, a possible model for the process is as follows:

- Calculate the solidus isotherm using heat-transfer theory. The equilibrium melting temperature can be assumed in the absence of a better estimate. This yields the width w and depth d, and area A_2.
- Calculate the volume of aluminium deposited per unit length, using (1). This corresponds to the cross-sectional area A_1. This apparently necessitates using a factor f, which corresponds to the fraction of powder alloyed.
- Calculate the height h of the weld bead above the original baseplate, assuming the reinforcement area A_1 adopts the shape of a spherical cap on the surface of the plate.
- Calculate the composition of the laser surface alloyed zone using equation (3).

The remaining problem is the determination of the solidus isotherm. The appropriate governing equations for the heat transfer problem are the energy equation

$$\frac{\partial T}{\partial t} + (u.\nabla)T = \kappa\nabla^2 T \tag{6}$$

the continuity equation

$$\nabla.u = 0 \tag{7}$$

and the momentum equation

$$\nabla.(uu) = -(1/\rho)\nabla p + \nu\nabla^2 u \tag{8}$$

where T is the temperature, t the time, u the velocity vector, κ the thermal diffusivity, p the pressure, ν the kinematic viscosity and ρ the density. Equations (6), (7) and (8) are subject to boundary conditions which are well documented in the literature (*e.g.* 15,16,17). As is well known, this set of equations represents a moving boundary problem. The position of the solid/liquid interface is not known *a priori*; it is to be determined, as boundary conditions apply at the interface.

In this work, equations (6), (7) and (8) have been discretised [15,16,17] for solution using the finite difference method; due to space limitations a more detailed write-up will be presented elsewhere. However, figure 7 illustrates typical calculations for the degenerate case of laser surface melting of titanium. A comparison of figure 7b and the experimental data tabulated in Table 1 shows that the model is capable of explaining the variation of melted zone dimensions with beam/substrate velocity. More work is required to extend the model to allow accurate prediction of compositions at high ratios of F/v.

7. Summary

Experimental data concerning the laser surface alloying of titanium substrates with aluminium have been rationalised. Analysis of the experimental data suggests that only 20% of the aluminium powder is successfully alloyed during the process, although this figure does not appear to vary significantly with velocity or feed rate. The observation that the aluminium composition is independent of velocity, at low ratios of feed rate/velocity has been explained. A model for the process in this feed rate/velocity regime has been established. It is recognised that more work is required to analyse the experimental data at high feed rate/velocity ratios, and this is where our attention will now be focussed.

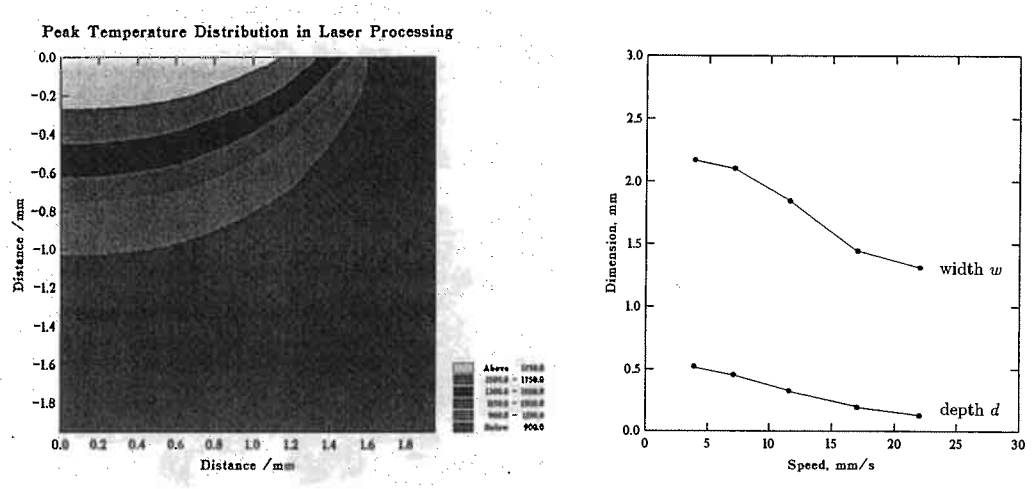

Figure 7: Left, a) Illustrative calculation of the temperature field during laser surface melting of titanium; Right, b) Calculated dimensions of laser melted zones of titanium, feed rate Al zero.

8. Acknowledgements

The authors would like to acknowledge the assistance of A. Camyab in determining some of the experimental data. H. Slinde performed the beam diagnostics experiments. It is a pleasure to acknowledge the technical support of A. Neve in the laser laboratory at Imperial College, and Professor Malcolm McLean for the provision of laboratory facilities.

9. References

[1.] J.C. Chesnutt and J.C. Williams, Metals and Materials, 509–511, (1990).
[2.] P.R. Munroe and I. Baker, Metals and Materials, 435–438, (1990).
[3.] H.A. Lipsitt, in Proc. MRS Symp, **39**, 351–364, (1985).
[4.] H.M. Flower, Private Communication, Imperial College, (1992).
[5.] G. Cam, H.M. Flower and D.R.F. West, Materials Science & Technology, **7**, 505–511, (1991).
[6.] S.M.L. Sastry and H.A. Lipsitt, Metall.. Trans., **8A**, 1543–1549, (1977).
[7.] J. Abboud and D.R.F. West, Materials Science and Technology, **7**, 827–834, (1991).
[8.] J. Abboud and D.R.F. West, Journal of Materials Science Letters, **9**, 308–310, (1990).
[9.] J. Abboud and D.R.F. West, Materials Science and Technology, **7**, 353–356, (1991).
[10.] Prometec GmbH: "Laserscope UFF100, lase beam diagnostic system for high power lasers, measurement of focused and unfocused beam, instructions for use", Aachen, Germany, (1990).
[11.] J.N. Clark, Materials Science and Technology, **1**, 1069–1080, (1985).
[12.] D. Rosenthal, Welding Journal Research Supplement, **20**, 220s–234s, (1941).
[13.] D. Rosenthal, Transactions ASME, **68**, 849–866, (1946).
[14.] N. Rykalin, A. Uglov and A. Kokova, 'Laser Machining and Welding', Chapter 3, Pergamon Press, Oxford, (1978).
[15.] C.W. Hirt, B.D. Nichols and N.C. Romero, Los Alamos Scientific Laboratory Report UC-34 and UC-79D, (1975).
[16.] C. Chan, J. Mazumder and M.M. Chen, Metallurgical Trans., **15A**, 2175–2184, (1984).
[17.] A. Paul and T. Debroy, in 'Advances in Welding Science and Technology', (edited S.A. David), ASM International, (1986).

Session 4
Sensing and Monitoring

4A. Detectors and Sensors

4B. In-Process Monitoring and Adaptive Control